Monthly Notices
of the
ROYAL ASTRONOMICAL SOCIETY

Mon. Not. R. Astron. Soc. **399,** 2021–2032 (2009) doi:10.1111/j.1365-2966.2009.15356.x

Monitoring supergiant fast X-ray transients with *Swift*: results from the first year

P. Romano,[1⋆] L. Sidoli,[2] G. Cusumano,[1] V. La Parola,[1] S. Vercellone,[1] C. Pagani,[3] L. Ducci,[2,4] V. Mangano,[1] J. Cummings,[5] H. A. Krimm,[5,6] C. Guidorzi,[7] J. A. Kennea,[3] E. A. Hoversten,[3] D. N. Burrows[3] and N. Gehrels[5]

[1]*INAF, Istituto di Astrofisica Spaziale e Fisica Cosmica, Via U. La Malfa 153, I-90146 Palermo, Italy*
[2]*INAF, Istituto di Astrofisica Spaziale e Fisica Cosmica, Via E. Bassini 15, I-20133 Milano, Italy*
[3]*Department of Astronomy and Astrophysics, Pennsylvania State University, University Park, PA 16802, USA*
[4]*Dipartimento di Fisica e Matematica, Università dell'Insubria, Via Valleggio 11, I-22100 Como, Italy*
[5]*NASA/Goddard Space Flight Center, Greenbelt, MD 20771, USA*
[6]*Universities Space Research Association, Columbia, MD 21044, USA*
[7]*Dipartimento di Fisica, Università di Ferrara, Via Saragat 1, I-44100 Ferrara, Italy*

Accepted 2009 July 7. Received 2009 July 7; in original form 2009 May 24

ABSTRACT

The advent of *Swift* has allowed, for the first time, the possibility to give supergiant fast X-ray transients (SFXTs), the new class of high-mass X-ray binaries discovered by the *International Gamma-Ray Astrophysics Laboratory*, non-serendipitous attention throughout most phases of their life. In this paper, we present our results based on the first year of intense *Swift* monitoring of four SFXTs, IGR J16479−4514, XTE J1739−302, IGR J17544−2619 and AX J1841.0−0536. We obtain the first assessment of how long each source spends in each state using a systematic monitoring with a sensitive instrument. The duty-cycle of inactivity is ∼17, 28, 39 and 55 per cent (∼5 per cent uncertainty), for IGR J16479−4514, AX J1841.0−0536, XTE J1739–302 and IGR J17544−2619, respectively, so that true quiescence, which is below our detection ability even with the exposures we collected in 1 yr, is a rare state, when compared with estimates from less sensitive instruments. This demonstrates that these transients accrete matter throughout their lifetime at different rates. AX J1841.0−0536 is the only source which has not undergone a bright outburst during our monitoring campaign. Although individual sources behave somewhat differently, common X-ray characteristics of this class are emerging, such as outburst lengths well in excess of hours, with a multiple peaked structure. A high dynamic range (including bright outbursts) of ∼4 orders of magnitude has been observed in IGR J17544−2619 and XTE J1739−302, of ∼3 in IGR J16479−4514 and of about 2 in AX J1841.0−0536 (this lowest range is due to the lack of bright flares). We also present a complete list of Burst Alert Telescope (BAT) on-board detections, which complements our previous work, and further confirms the continuous activity of these sources. We performed out-of-outburst intensity-based spectroscopy. In particular, spectral fits with an absorbed blackbody always result in blackbody radii of a few hundred metres, consistent with being emitted from a small portion of the neutron star surface, very likely the neutron star polar caps. We used the whole BAT data set, since the beginning of the mission, to search for periodicities due to orbital motion and found $P_{\rm orb} = 3.32$ d for IGR J16479−4514, confirming previous findings. We also present the Ultraviolet/Optical Telescope (UVOT) data of these sources; we show the UVOT light curves of AX J1841.0−0536 and the ones of XTE J1739−302 before, during and after the outbursts.

Key words: X-rays: binaries – X-rays: individual: IGR J16479−4514 – X-rays: individual: XTE J1739–302 – X-rays: individual: IGR J17544−2619 – X-rays: individual: AX J1841.0−0536.

1 INTRODUCTION

Supergiant fast X-ray transients (SFXTs) are a subclass of high-mass X-ray binaries (HMXBs) recently discovered by the

⋆E-mail: romano@ifc.inaf.it

© 2009 The Authors. Journal compilation © 2009 RAS

Downloaded from http://mnras.oxfordjournals.org/ at NASA Goddard Space Flight Ctr on July 1, 2014

International Gamma-Ray Astrophysics Laboratory (*INTEGRAL*) during the Galactic plane monitoring (Sguera et al. 2005). They are firmly associated (via optical spectroscopy) with an O or B supergiant and display outbursts which are significantly shorter than typical Be/X-ray binaries, characterized by bright flares with a duration of a few hours and peak luminosities of 10^{36}–10^{37} erg s^{-1}. The quiescence, characterized by a soft spectrum (likely thermal) and a low luminosity at $\sim 10^{32}$ erg s^{-1} is a rarely observed state (e.g. in't Zand 2005). As their spectral properties resemble those of accreting pulsars, it is generally assumed that all members of the new class are HMXBs hosting a neutron star, although the only three SFXTs with a measured pulse period are AX J1841.0−0536 ($P_{\rm spin} \sim 4.7$ s; Bamba et al. 2001), IGR J11215–5952 ($P_{\rm spin} \sim 187$ s; Swank, Smith & Markwardt 2007) and IGR J18483–0311 ($P_{\rm spin} \sim 21$ s; Sguera et al. 2007). The mechanisms responsible for the observed short outbursts are still being debated. The proposed explanations (see Sidoli 2009, for a recent review) mainly involve the structure of the wind from the supergiant companion (in't Zand 2005; Sidoli et al. 2007; Walter & Zurita Heras 2007; Negueruela et al. 2008), or the possible presence of gated mechanisms (see Bozzo, Falanga & Stella 2008a). The latter are due to the properties of the accreting neutron star (magnetar-like magnetic fields and slow pulse periods) which can halt the accretion for most of the time.

During 2007 February, we monitored the outburst of the periodic SFXT IGR J11215−5952 (Romano et al. 2007; Sidoli et al. 2007) with *Swift* (Gehrels et al. 2004), in what became the most complete and deep set of X-ray observations of an outburst of a SFXT. Thanks to these observations, we discovered that the accretion phase during the bright outburst lasts much longer than a few hours. The orbital dependence of the accretion X-ray luminosity during the outburst led us to propose an alternative explanation for the outburst mechanism in IGR J11215−5952 (Sidoli et al. 2007), linked to the possible presence of a second wind component, in the form of a preferred plane for the outflowing wind from the supergiant donor. X-ray outbursts should be produced when the neutron star crosses this density enhanced wind component.

Following the success of the *Swift* observations on IGR J11215–5952, we extended the investigation to a small although well-defined sample of SFXTs. *Swift* was the most logical choice to monitor the light curves of our sample, because of its unique fast-slewing and flexible observing scheduling, which makes a monitoring effort cost-effective, its broad-band energy coverage that would allow us to model the observed spectra simultaneously in the 0.3–150 keV energy range, thus testing the prevailing models for accreting neutron stars, and the high sensitivity in the soft X-ray regime, where some of the SFXTs had never been observed.

In Sidoli et al. (2008, Paper I),we described the long-term X-ray emission outside the bright outbursts based on the first 4 months of data; in Romano et al. (2008c, Paper II) and Sidoli et al. (2009b, Paper III), we reported on the outbursts of IGR J16479−4514, and the prototypical IGR J17544−2619 and XTE J17391−302, respectively, while in Sidoli et al. (2009a, Paper IV) we report the results of more outbursts of XTE J1739−302 and IGR J17544−2619. In this paper, we draw a general picture of our knowledge on SFXT, by summarizing the results on the outbursts caught by *Swift* during the first year of our ongoing campaign, and report on the X-ray Telescope (XRT; Burrows et al. 2005) and Ultraviolet/Optical Telescope (UVOT; Roming et al. 2005) data collected from 2007 October 26 to 2008 November 15, as well as the Burst Alert Telescope (BAT; Barthelmy et al. 2005) data collected since the start of the mission. We also include data from the 2009 January 29 outburst of IGR J16479−4514 (Romano et al. 2009b).

2 OUR SAMPLE AND OBSERVATIONS

The four targets, IGR J16479−4514, XTE J1739–302, IGR J17544−2619 and AX J1841.0−0536, were selected by considering sources which, among several SFXT candidates, are confirmed SFXTs, i.e. they display both a 'short' transient (and recurrent) X-ray activity and they have been optically identified with supergiant companions (see Walter & Zurita Heras 2007, and references therein). XTE J1739–302 and IGR J17544−2619, in particular, are generally considered prototypical SFXTs: XTE J1739–302 was the first transient which showed an unusual X-ray behaviour (Smith et al. 1998), only recently optically associated with a blue supergiant (Negueruela et al. 2006). AX J1841.0−0536/IGR J18410−0535, was chosen because at the time it was the only SFXT, together with IGR J11215–5952, where a pulsar had been detected (Bamba et al. 2001). Finally, IGR J16479−4514 had displayed in the past a more frequent X-ray outburst occurrence than other SFXTs (see e.g. Walter & Zurita Heras 2007), and offered an a priori better chance to be caught during an outburst.

For these sources, we obtained two to three observations week^{-1} object^{-1}, each 1 ks long with XRT in AUTO mode, to best exploit XRT automatic mode switching (Hill et al. 2005) in response to changes in the observed fluxes. This observing pace would naturally fit in the regular observation scheduling of gamma-ray bursts (GRBs), which are the main observing targets for *Swift*. We also proposed for further target of opportunity (ToO) observations whenever one of the sources showed interesting activity, (such as indications of an imminent outburst) or underwent an outburst, thus obtaining a finer sampling of the light curves and allowing us to study all phases of the evolution of an outburst.

During the first year, we collected a total of 330 *Swift* observations as part of our program, for a total net XRT exposure of ∼363 ks accumulated on all sources and distributed as shown in Table 1.

In this paper, we also include the data on the 20 d campaign (for a total on-source time of ∼34 ks) on IGR J16479−4514, which triggered the BAT on 2009 January 29 at 06:33:07 UT (image trigger = 341 452, Romano et al. 2009b). *Swift* slewed to the target so that the XRT started observing the field at 06:46:46.9 UT, 819.3 s after the BAT trigger. The BAT transient monitor showed enhanced emission (in excess of 20 mCrab) from 01:38:56 to 07:02:08 UT. During the image trigger interval (the 640 s starting on 2009 January 29 at 06:27:5) the rate was 0.022 ± 0.003 counts s^{-1} (97 mCrab). IGR J16479−4514 showed renewed activity on 2009 February 8, starting from about 20:30 UT (La Parola et al. 2009). For the 504 s pointing starting on 2009 February 08 at 20:30 UT the BAT transient monitor rate was 0.019 ± 0.003 counts s^{-1} (85 mCrab).

3 DATA REDUCTION

The XRT data were uniformly processed with standard procedures (XRTPIPELINE v0.11.6), filtering and screening criteria by using FTOOLS in the HEASOFT package (v.6.4). We considered both windowed timing (WT) and photon counting (PC) data, and selected event grades 0–2 and 0–12, respectively (Burrows et al. 2005). When appropriate, we corrected for pile-up by determining the size of the point spread function (PSF) core affected by comparing the observed and nominal PSF (Vaughan et al. 2006), and excluding from the analysis all the events that fell within that region. We used the spectral redistribution matrices v010 in the HEASARC Calibration Database (CALDB).

Downloaded from http://mnras.oxfordjournals.org/ at NASA Goddard Space Flight Ctr on July 1, 2014

Table 1. Summary of the *Swift*/XRT monitoring campaign of the four SFXTs during the first year.

Name	Campaign start (yyyy-mm-dd)	Campaign end (yyyy-mm-dd)	N^a	Exposure^b (ks)	Outburst^c dates (yyyy-mm-dd)	BAT trigger	References
IGR J16479−4514	2007-10-26	2008-10-25	70	75.2	2008-03-19	306 829	Romano et al. (2008c)
					2008-05-21	312 068	
					2009-01-29	*341 452*	*Romano et al. (2009b), La Parola et al. (2009)*
XTE J1739−302	2007-10-27	2008-10-31	95	116.1	2008-04-08	308 797	Sidoli et al. (2009b)
					2008-08-13	319 963	Romano et al. (2008b), Sidoli et al. (2009a)
					2009-03-10	*346 069*	*Romano et al. (2009a)*
IGR J17544−2619	2007-10-28	2008-10-31	77	74.8	2007-11-08		Krimm et al. (2007)
					2008-03-31	308 224	Sidoli et al. (2009b)
					2008-09-04		Romano et al. (2008a), Sidoli et al. (2009a)
					2009-03-15		*Krimm, Romano & Sidoli (2009)*
AX J1841.0−0536	2007-10-26	2008-10-15	88	96.5	None		
Total			330	362.6			

[a]Number of observations obtained during the monitoring campaign.
[b]*Swift*/XRT net exposure.
[c]BAT trigger dates.
Note. We report the outbursts that occurred in 2009 in italics, for the sake of completeness.

We retrieved the BAT orbit-by-orbit light curves (15–50 keV) covering the data range from 2005 February 12 to 2008 December 31 (MJD range 53413–54831) from the BAT transient monitor (Krimm et al. 2006, 2008) page.[1]

The UVOT observed the four targets simultaneously with the XRT with the 'Filter of the Day', i.e. the filter chosen for all observations to be carried out during a specific day in order to minimize the filter wheel usage. The only exceptions are the observations during outbursts, when all filters were used in the typical GRB sequence (Roming et al. 2005). The data analysis was performed using the UVOTIMSUM and UVOTSOURCE tasks included in the FTOOLS software. The latter task calculates the magnitude through aperture photometry within a circular region and applies specific corrections due to the detector characteristics. The reported magnitudes are on the UVOT photometric system described in Poole et al. (2008), and are not corrected for Galactic extinction. At the position of IGR J16479−4514, no detection was achieved down to a limit of $u = 21.07$ mag. For IGR J17544−2619, only engineering data were collected, as is generally the case for a field which contains a source too bright to be observed; the only exceptions were the outburst segments 00308224000, and the two following it, 00035056021 and 00035056023 (see Table 7, and Paper III), where we observe $v = 12.8$ mag and $uvw2 = 18.13 \pm 0.05$ and 18.00 ± 0.06 mag, respectively.

All quoted uncertainties are given at 90 per cent confidence level for one interesting parameter unless otherwise stated. The spectral indices are parametrized as $F_\nu \propto \nu^{-\alpha}$, where F_ν (erg cm^{-2} s^{-1} Hz^{-1}) is the flux density as a function of frequency ν; we adopt $\Gamma = \alpha + 1$ as the photon index, $N(E) \propto E^{-\Gamma}$ (ph cm^{-2} s^{-1} keV^{-1}).

4 TIMING

4.1 XRT inactivity duty cycle

Fig. 1 shows the XRT light curves collected from 2007 October 26 to 2008 November 15, in the 0.2–10 keV band, which were corrected for pile-up, PSF losses and vignetting, and background-subtracted. Each point in the light curves refers to the average flux observed during each observation performed with XRT; the exceptions are the outbursts (listed in Table 1) where the data were binned to include at least 20 source counts per time bin to best represent the count rate dynamical range. Due to the sources being Sun-constrained between roughly 2007 December and 2008 January, depending on the target coordinates, no data were collected during those months.

Given the structure of the observing plan, we can realistically consider our monitoring as a casual sampling of the light curve at a resolution of about ∼4 d. Therefore, we can calculate the percentage of time each source spent in each relative flux state. In order to do this, we divided the observations into three states, namely (i) BAT-detected outburst, (ii) intermediate state (all observations yielding a firm detection excluding outburst ones) and (iii) 'non-detections' (detections with a significance below 3σ). Since a few observations were interrupted by GRB events, the consequent non-detection may be due to the short exposure, not exclusively to the source being faint. Therefore, to create a uniform subsample for the latter state, we excluded all observations that had a net exposure below 900 s.

An exposure of 900 s corresponds to 2–10 keV flux limits that vary between 1 and 3×10^{-12} erg cm^{-2} s^{-1} (3σ), depending on the source. These values were derived from a measurement of the local background and a count rate to flux conversion calculated by using the best fit absorbed power-law models of the 'low' (or 'medium' if 'low' was not available) state in Table 4.

We define as *duty cycle of inactivity*, the time each source spends *undetected* down to a flux limit of 1–3 $\times 10^{-12}$ erg cm^{-2} s^{-1},

$$\mathrm{IDC} = \Delta T_\Sigma / [\Delta T_{\rm tot}\,(1 - P_{\rm short})],$$

where ΔT_Σ is sum of the exposures accumulated in all observations, each in excess of 900 s, where only a 3σ upper limit was achieved (Table 2, Column 5), $\Delta T_{\rm tot}$ is the total exposure accumulated (Table 1, Column 5) and $P_{\rm short}$ is the percentage of time lost to short observations (exposure <900 s, Table 2, Column 6). We obtain that IDC ∼ 17, 28, 39, 55 per cent, for IGR J16479−4514, AX J1841.0−0536, XTE J1739–302 and IGR J17544−2619, respectively (Table 2, Column 7). We estimate an error of ∼5 per cent on these values.

We accumulated all data for which no detections were obtained as single exposures (whose total exposure is ΔT_Σ), and performed a

[1] http://swift.gsfc.nasa.gov/docs/swift/results/transients/

© 2009 The Authors. Journal compilation © 2009 RAS, MNRAS **399,** 2021–2032

Downloaded from http://mnras.oxfordjournals.org/ at NASA Goddard Space Flight Ctr on July 1, 2014

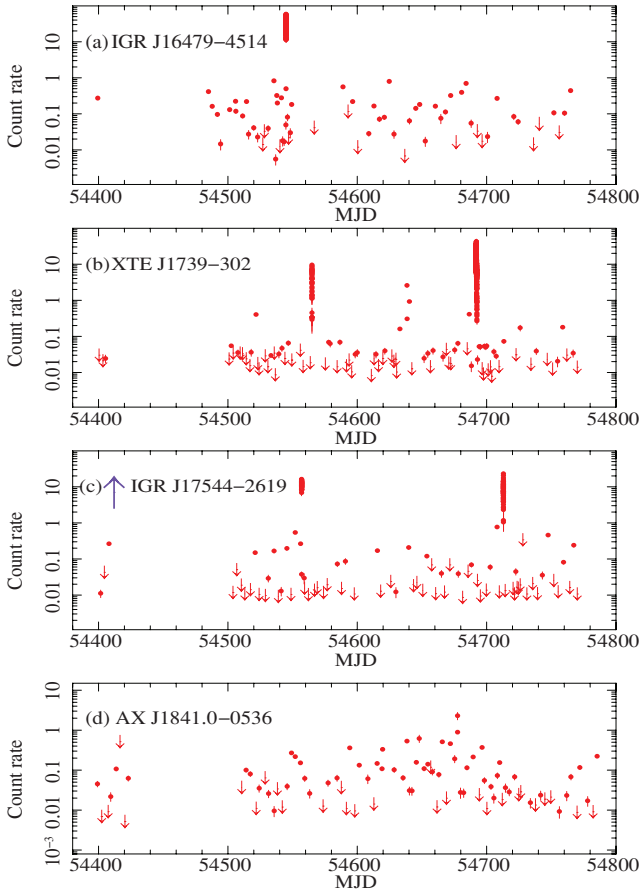

Figure 1. *Swift*/XRT (0.2–10 keV) light curves, corrected for pile-up, PSF losses, vignetting and background-subtracted. The data were collected from 2007 October 26 to 2008 November 15. The downward-pointing arrows are 3σ upper limits. The upward pointing arrow marks an outburst that triggered the BAT on MJD 54414, but which could not be followed by XRT because the source was Sun-constrained for the XRT.

detection. The resulting cumulative mean count rate for each object is reported in Table 2 (Column 8).

4.2 BAT on-board detections

In Table 3, we list the BAT on-board detections in the 15–50 keV band. If an alert was generated, a BAT trigger was assigned (Columns 4 and 8) and notes were disseminated.[2] For some of these triggers a burst response [slew and repointing of the narrow field instruments (NFI)] was also initiated, depending on GRB observing load, observing constraints and interest in the sources. More details on several of these triggers can be found in the papers of our series (see Table 1 for references). These data show that the four sources are quite active even outside the outbursts, not only when observed by XRT but also by BAT.

4.3 Searching for orbital periodicities in BAT data

We looked for evidence of orbital periodicities in the BAT data. We first considered the BAT data for the four sources binned orbit-by-orbit in the time range MJD 53413–54829. These data were further screened to exclude bad quality points (quality flag 1 and 2) and referred to the Solar system barycentre (SSB) by using the task EARTH2SUN.

A folding technique was applied to the baricentred arrival times by searching in the 0.1–50 d period range and by building 16 bin pulse profiles with a step given by $P^2/(N\Delta T)$, where N is the number of phase bins and ΔT is the data span length. We find significant evidence for orbital modulation for IGR J16479–4514 with a best period of 286 792 ± 42 s ($P_{\rm orb}$ = 3.3193 ± 0.0005 d) referred to the epoch time MJD 54170.205 002 13, with a χ^2 value of 155.8. As shown in the periodogram in Fig. 2(a), this periodicity stands out from the noise and is certainly not due to the satellite orbital period or its multiples, as instead is the case for the peaks appearing below 1 d. Peaks at periods higher than 5 d are multiples of the $P_{\rm orb}$. A zoomed-in region of the periodogram around the candidate $P_{\rm orb}$ is shown in Fig. 2(b). The statistics of the data is not Gaussian, so assessment of the significance of this periodicity needs to be performed on the noise distribution of χ^2 in the periodogram. Fig. 2(c) represents the noise distribution of the powers of the periodogram after removal of the satellite orbital data period (and its multiples), and of the multiples of $P_{\rm orb}$. In order to evaluate the significance of the signal at $P_{\rm orb}$, we fit the distribution for $25 < \chi^2 < 80$ with an exponential function and evaluated the integral of the best-fitting function beyond the value of the χ^2 obtained at $P_{\rm orb}$. This integral yields a number of chance occurrences due to noise of 1.24×10^{-5}, corresponding to 4.5 standard deviations in Gaussian statistics. In Fig. 2(d), we show the pulsed profile folded at $P_{\rm orb}$. There is clear evidence for an eclipse phase, whose epoch centroid, evaluated by fitting the data around the dip with a Gaussian function, is MJD 54171.11 ± 0.05. This confirms the results of Jain, Paul & Dutta (2009).

Adopting the same techniques for XTE J1739–302 (Fig. 3a), we find marginal evidence for a signal above the noise at 1 111 605.1 ± 631.3 s ($P_{\rm orb}$ = 12.8658 ± 0.0073 d) with a χ^2 value of 94.7. The second highest peak in Fig. 3(a) is the first multiple of $P_{\rm orb}$. The chance probability to obtain this signal at $P_{\rm orb}$ is 3.1×10^{-2}, corresponding to 2.1 standard deviations in Gaussian statistics. By repeating this kind of analysis on 1/4, 1/2, 3/4 and the whole BAT data sample, we verified that the power at this $P_{\rm orb}$ increases with time baseline, as is expected of signal, as opposed to noise. This strengthens the possibility that this is a true periodicity.

No significant evidence for orbital periodicity was found for either IGR J17544−2619 or AX J1841.0−0536.

4.4 Searching for spin periodicities in XRT data

We also looked for evidence of spin periodicities in XRT data. For each source, we performed a timing analysis to search for coherent pulsations within *each single observation* with a slow Fourier analysis on the fundamental harmonics in the 0.0047–0.199 418 Hz frequency range (the latter being the Nyquist frequency of the data set, corresponding to a period of 5.014 60 s), with the frequency resolution $df = 1/(2\Delta T)$ Hz, where ΔT is the length of each observation. As the expected power of the pulsed emission is $P_i = K \times F_{\rm P}^2 \times N_t + 2$, we only used observations with a minimum statistic content $N_t > 300$ counts, that would yield a detection with a significance greater than 3 standard deviations for a signal with a pulsed fraction of $F_{\rm P} = 0.2$, and $K = 0.5$ (sinusoidal profile). No significant deviations from a statistically flat distribution was revealed in the Fourier spectra of these observations.

In order to reveal the presence of a pulsed signal that could be undetectable in single observations because of the poor statistics, we performed a *stacked timing analysis* on a larger set of

[2] http://gcn.gsfc.nasa.gov/gcn/swift_grbs.html

Downloaded from http://mnras.oxfordjournals.org/ at NASA Goddard Space Flight Ctr on July 1, 2014

Table 2. Duty cycle of inactivity of the four SFXTs.

Name	Limiting rate[a] (0.2–10 keV) (10^{-3} counts s^{-1})	Limiting $F^{a,b}$ (2–10 keV) (10^{-12} erg cm^{-2} s^{-1})	Limiting $L^{a,b}$ (2–10 keV) (10^{35} erg s^{-1})	ΔT_Σ (ks)	$P_{\rm short}$ (per cent)	IDC (per cent)	Rate$_{\Delta T_\Sigma}$ (0.2–10 keV) (10^{-3} counts s^{-1})
IGR J16479−4514	16	2.4	0.62	12.2	2	17	2.9 ± 0.7
XTE J1739−302	13	1.6	0.13	40.3	9	39	3.9 ± 0.4
IGR J17544−2619	13	1.2	0.17	37.0	10	55	1.9 ± 0.3
AX J1841.0−0536	13	1.7	0.45	26.6	3	28	2.4 ± 0.4

Note. Count rates are in units of 10^{-3} counts s^{-1} in the 0.2–10 keV energy band. Observed fluxes and luminosities are in units of 10^{-12} erg cm^{-2} s^{-1} and 10^{35} erg s^{-1} in the 2–10 keV energy band, respectively. ΔT_Σ is the sum of the exposures accumulated in all observations, each in excess of 900 s, where only a 3σ upper limit was achieved; $P_{\rm short}$ is the percentage of time lost to short observations; IDC is the *duty cycle of inactivity*, the time each source spends undetected down to a flux limit of 1–3 $\times$ 10^{-12} erg cm^{-2} s^{-1}; rate$_{\Delta T_\Sigma}$ is detailed in the text (Section 4.1).
[a]Based on a single 900 s exposure.
[b]Based on the best-fitting model for the 'low' (or 'medium' if 'low' unavailable) absorbed power-law model in Table 4.

Table 3. BAT on-board detections in the 15–50 keV band.

MJD	Date	Time[a]	BAT trigger N.[b]	S/N[c]	MJD	Date	Time[a]	BAT trigger N.[b]	S/N[c]
		IGR J16479−4514					XTE J1739−302		
53612	2005-08-30	04:03:28–04:13:52	152 652 (NFI)	7.71	53581	2005-07-30	00:23:12–00:28:56		
53811	2006-03-17	08:03:51			53663	2005-10-20	12:53:04		
53875	2006-05-20	17:32:39–17:35:51	210 886 (no slew)	5.78	53765	2006-01-30	18:33:43–20:26:15		
53898	2006-06-12	06:58:31			53798	2006-03-04	04:52:31		
53910	2006-06-24	20:19:59	215 914 (no slew)	5.34	53806	2006-03-12	07:13:27		
54095	2006-12-26	22:39:43–22:45:03			54140	2007-02-09	17:33:03–17:34:07		
54167	2007-03-08	06:04:55			54161	2007-03-02	13:39:11–15:05:27	[d]	
54196	2007-04-06	15:22:55			54168	2007-03-09	11:09:51–11:14:47	[d]	
54239	2007-05-19	19:53:59–20:04:39			54269	2007-06-18	03:09:43–03:10:47	282535 (no slew)	6.53
54310	2007-07-29	12:07:35	286 412 (no slew)	9.98	54411	2007-11-07	04:38:15–04:42:31		
54320	2007-08-08	21:13:51			54564	2008-04-08	16:43:19–21:28:15	308797 (NFI)	7.83
54368	2007-09-25	18:14:31			54565	2008-04-09	00:45:11–00:51:35		
54506	2008-02-10	05:35:43			54632	2008-06-15	06:56:39		
54535	2008-03-10	13:11:03–13:20:39			54673	2008-07-26	14:13:27		
54544	2008-03-19	22:44:47–22:59:59	306 829 (NFI)	12.02[e]	54691	2008-08-13	23:49:19–23:51:27	319963 (NFI)	9.15
54572	2008-04-16	17:07:11			54692	2008-08-14	00:04:23–03:06:39	319964 (NFI)	11.14
54607	2008-05-21	06:03:43–15:38:23	312 068 (no slew)	7.21	54724	2008-09-15	12:59:59–13:06:23		
54664	2008-07-17	18:10:15			54900	2009-03-10	18:18:38–18:39:58	346069 (NFI)	6.81
54679	2008-08-01	03:38:31–03:49:03							
54682	2008-08-04	04:06:55–04:14:39							
54687	2008-08-09	01:11:51							
54826	2008-12-26	15:55:11–15:57:19							
54860	2009-01-29	06:32:06–06:48:14	341 452 (NFI)	10.68					
		IGR J17544−2619					AX J1841.0−0536		
53996	2006-09-18	09:07:43			53821	2006-03-27	00:51:03–08:39:27	202892 (no slew)	5.45
53998	2006-09-20	11:11:43	[f]		53834	2006-04-09	16:33:43		
54009	2006-10-01	10:34:47			53845	2006-04-20	14:42:31		
54035	2006-10-27	00:33:11			54026	2006-10-18	10:50:23		
54372	2007-09-29	13:21:51–16:36:55			54053	2006-11-14	10:21:19		
54387	2007-10-14	00:39:35–19:57:27			54139	2007-02-08	22:21:59		
54412	2007-11-08	01:31:03–06:16:47			54195	2007-04-05	12:00:31		
54556	2008-03-31	20:50:47	308 224 (NFI)	9.10					
54565	2008-04-09	18:17:19							
54611	2008-05-25	14:43:51–14:55:03							

[a]Time of the start of the BAT trigger, or the time range when on-board detections were obtained.
[b]BAT regular trigger, as was disseminated through GCNs. NFI indicates that there are data from the narrow-field instrument; no slew, indicates that *Swift* did not slew to the target.
[c]On-board image significance in units of σ.
[d]Also reported by Blay et al. (2008).
[e]Trigger 306830 had S/N = 21.64, see Romano et al. (2008c).
[f]Also reported by Ducci et al. (2008).

Downloaded from http://mnras.oxfordjournals.org/ at NASA Goddard Space Flight Ctr on July 1, 2014

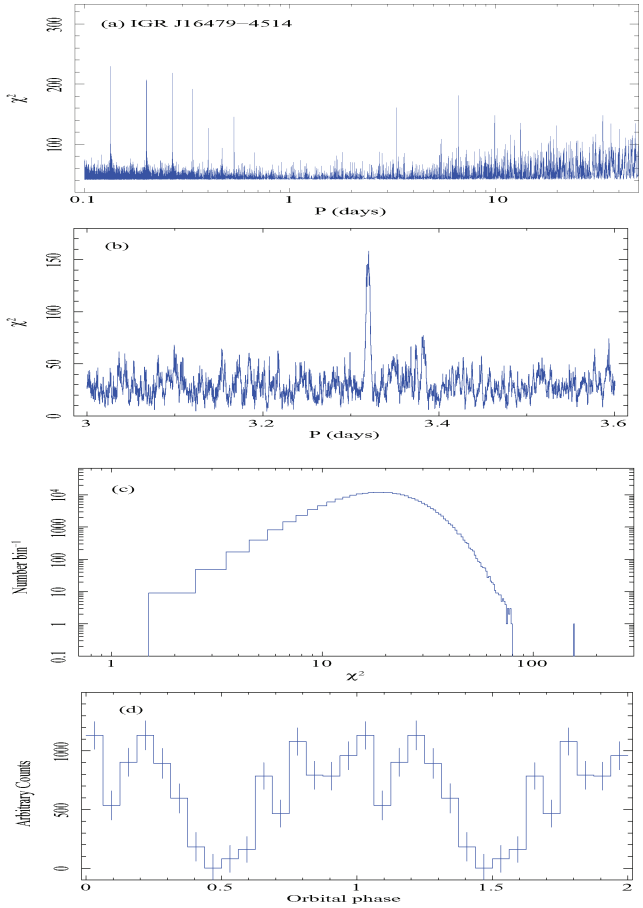

Figure 2. (a) Periodogram of *Swift*/BAT (15–50 keV) data for IGR J16479–4514 (MJD range 53413–54829) from the BAT transient monitor in the whole time range examined. (b) Close-up around the $P = 3.32$ d periodicity. (c) Distribution of χ^2 values. (d) Light curve folded at a period $P = 3.32$ d, with 16 phase bins.

observations. This analysis consists in summing the power spectra obtained from single observations with a common frequency range (0.005–0.2 Hz) and resolution $1/2\Delta T_{\rm max}$, where $\Delta T_{\rm max}$ is the elapsed time of the longest observation. The averaged power spectrum will have a distribution with mean 2 and standard deviation $2/\sqrt{N}$, where N is the number of summed power spectra. However, we cannot add arbitrarily long amounts of data without taking into account the Doppler modulation due to orbital motion which could destroy the coherence of the pulsed signal. For IGR J16479–4514, for which a firm detection of a $P_{\rm orb}$ was obtained, we could minimize the effect of the orbital Doppler modulation, by summing the spectra which are close in orbital phase. Under the simplifying assumption of a circular orbit, we evaluated the orbital phase for each XRT observation and divided the sample in four phase intervals: 0.85–0.15, 0.15–0.35, 0.35–0.65 and 0.65–0.85. The different amplitudes were chosen to take into account the different values of the tangential velocity of the compact object along its orbit. In the four stacked spectra, we found no evidence for a significant excess above the noise distribution.

4.5 Searching for eclipses in IGR J16479−4514 XRT data

The data of the whole XRT campaign on IGR J16479−4514 were sought for the presence of eclipses, suggested by Bozzo et al. (2008b) on the basis of the analysis of an *XMM–Newton* observation. We created event lists for the whole campaign and selected those inside and outside the eclipses, where by 'inside the eclipse' we consider the time interval between the start of the eclipse as defined by Bozzo et al. (2008b) and 0.6 d later [using the ephemeris from Jain et al. (2009)]. We then calculated the net (subtracted for scaled background) count rate in the two cases. We obtain $(6 \pm 1) \times 10^{-3}$ counts s^{-1} (inside) and 0.169 ± 0.002 counts s^{-1} (outside). Consistent values [$(6 \pm 3) \times 10^{-3}$ and 0.203 ± 0.003 counts s^{-1}, respectively] are measured during the 2009 January outburst. This indicates that the source is in two distinct flux levels inside and outside the predicted times of the eclipses at the $\sim 50\sigma$ level. We also calculated the count rates within individual time slices inside eclipses and find that they never exceed 0.013 counts s^{-1}. We can thus conclude that the XRT data are consistent with the presence of an eclipse on the longest baseline so far examined. In particular, Fig. 4 shows the light curve of IGR J16479−4514 during the 2009 January 29 outburst with vertical lines marking the predicted positions of the eclipse times.

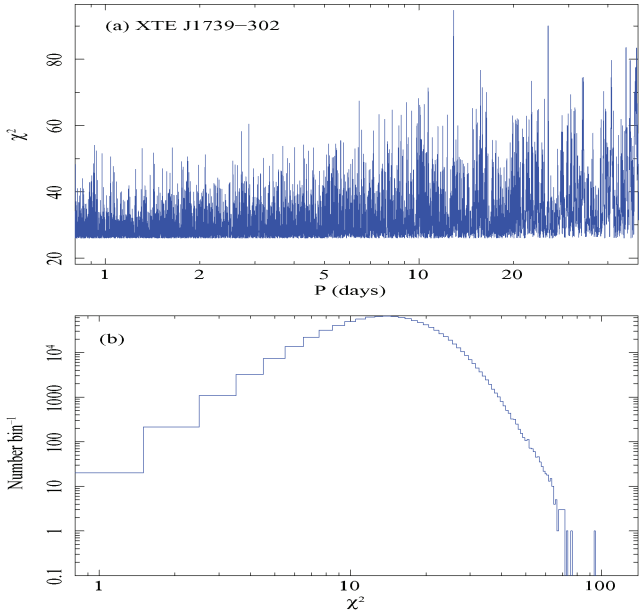

Figure 3. (a) Periodogram of *Swift*/BAT (15–50 keV) data for XTE J1739–302 (MJD range 53413–54829) from the BAT transient monitor in the whole time range examined. (b) Distribution of χ^2 values.

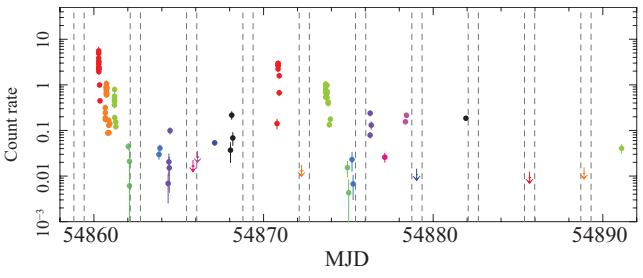

Figure 4. XRT light curve of the *Swift*/XRT observations after the 2009 January 29 outburst of IGR J16479−4514 in the 0.3–10 keV band, background-subtracted and corrected for pile-up, PSF losses and vignetting. Different colours denote different observations. Filled circles are full detections (S/N > 7), while downward-pointing arrows are 3σ upper limits. The vertical lines mark the predicted positions of the eclipse.

Downloaded from http://mnras.oxfordjournals.org/ at NASA Goddard Space Flight Ctr on July 1, 2014

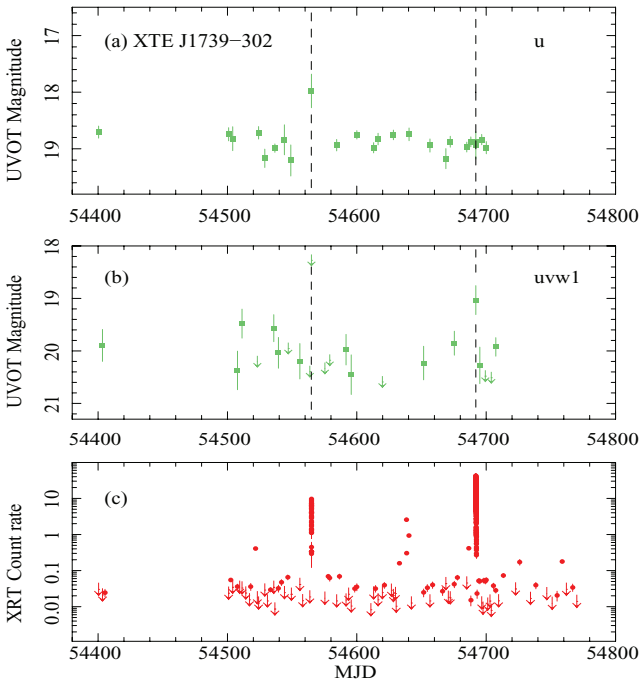

Figure 5. Light curves of XTE J1739–302. (a) *Swift*/UVOT u light curve; (b) *Swift*/UVOT $uvw1$ light curve; (c) *Swift*/XRT light curve. The vertical dashed lines mark the BAT outbursts.

4.6 UVOT light curves

We report for the first time on optical/UV observations performed with UVOT simultaneously to our *Swift*/XRT monitoring of the SFXTs. In Figs 5(a) and (b), we show the UVOT u and $uvw1$ light curves of XTE J1739−302 of the whole campaign. The dashed vertical lines mark the two X-ray outbursts (2008 April 8, 2008 August 13; Fig. 5b). The ultraviolet filters only registered upper limits for this source during the outbursts. We consider the correspondence between the X-ray peak and the u magnitude. During the first outburst, the u band shows an increase of ∼0.9 mag with respect to the campaign mean or a factor of ∼2.5 in flux. Depending on the choice of background regions, this is a 2–3σ effect. During the second outburst, the u magnitude is consistent with the mean for the whole campaign; the b and v magnitudes, collected as part of the GRB-chasing filter scheme, show the same level as in the first one. The $uvw1$ magnitudes show a larger degree of variability when compared with the u band. We also investigated intra-day variability during the outbursts, but found no significant variation within the errors in all bands.

In Figs 6(a)–(c), we show the UVOT u and $uvw1$, and $uvw2$ light curves of AX J1841.0−0536. The u and $uvw1$ are remarkably stable, while the $uvw2$ show some degree of variability. We note that the highest point in the $uvw2$ light curve is not simultaneous with the X-ray peak.

5 X-RAY SPECTROSCOPY

5.1 The 2009 January 29 outburst of IGR J16479−4514

In response to the 2009 January 29 outburst of IGR J16479−4514, *Swift* performed a delayed slew, so that the NFI were on target >800 s after the trigger (Romano et al. 2009b). At this point, the flux registered by the BAT was rather low, and meaningful broad-band

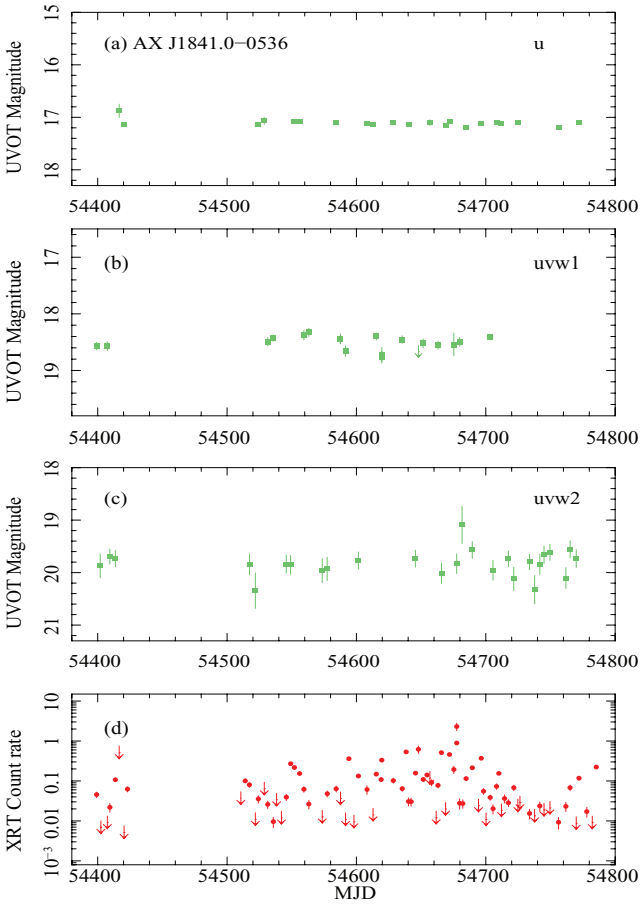

Figure 6. Light curves of AX J1841.0−0536. (a) *Swift*/UVOT u magnitudes; (b) *Swift*/UVOT $uvw1$ magnitudes; (c) *Swift*/XRT $uvw2$ magnitudes; (d) *Swift*/XRT light curve.

(XRT+BAT) spectroscopy is not possible, given the 107 s overlap in the observations. Therefore, here we only report the fits to the XRT data. An absorbed power-law model yielded an absorbing column of $N_{\rm H} = (7.1^{+2.6}_{-2.0}) \times 10^{22}$ cm^{-2}, a photon index $\Gamma = 1.6 \pm 0.5$, and an unabsorbed flux in the 2–10 keV band is 2×10^{-10} erg cm^{-2} s^{-1}. The X-ray spectrum extracted from segment 00030296087, when the source showed rebrightening (La Parola et al. 2009), was also fit with an absorbed power-law model, obtaining $\Gamma = 1.3 \pm 0.5$, $N_{\rm H} = (7.1^{+2.6}_{-2.0}) \times 10^{22}$ cm^{-2} and unabsorbed flux in the 2–10 keV band of 3×10^{-10} erg cm^{-2} s^{-1}. These results are generally consistent with the ones found in Paper II, which describes the outburst of this source which occurred on 2008 March 19, 315 d earlier. We also note that, as found in Paper II, the derived $N_{\rm H}$ is in excess of the one along the line of sight, 1.87×10^{22} cm^{-2}. The broad-band spectroscopy of the other outbursts caught during the campaign has already been reported on elsewhere (Papers II, III and IV; see Table 1) and we will also summarize them below.

5.2 Out-of-outburst X-ray spectroscopy

In the remainder of this section, we concentrate on the out-of-outburst emission. To characterize the spectral properties of the sources in several states, we accumulated the events in each observation when the source was not in outburst and a detection was achieved. For these events, we estimated from the light curves (binned at a 100 s resolution) three count rate levels, CR_1, CR_2 and CR_3 (reported in Table 4) that would yield comparable statistics

Downloaded from http://mnras.oxfordjournals.org/ at NASA Goddard Space Flight Ctr on July 1, 2014

Table 4. XRT spectroscopy of the four SFXTs (2007+2008 data set).

Name Absorbed power law	Spectrum	Rate (counts s^{-1})	N_H (10^{22} cm^{-2})	Parameter Γ	Hardness[a] ratio	Flux[b] (2–10 keV)	Luminosity[c] (2–10 keV)	χ^2_{red}/dof[d] Cstat (per cent)
IGR J16479−4514	High	>0.52	$7.0^{+0.8}_{-0.7}$	$1.2^{+0.2}_{-0.2}$		120	5	1.1/131
	Medium	[0.25–0.52]	$9.3^{+1.1}_{-1.0}$	$1.5^{+0.2}_{-0.2}$		54	3	1.0/132
	Low	[0.06–0.25]	$6.7^{+0.7}_{-0.7}$	$1.4^{+0.2}_{-0.2}$		19	0.8	0.9/144
	Very low[e]	<0.06	$3.3^{+1.4}_{+0.0}$	$1.5^{+0.5}_{-0.4}$		1.8	0.04	482.3 (89.3)
	Very low[f]	<0.06	$0.3^{+0.6}_{-0.3}$	$0.3^{+0.5}_{-0.4}$	0.9 ± 0.3	1.8	0.05	471.5 (50.2)
XTE J1739−302	High	>0.33	$2.7^{+0.5}_{-0.4}$	$0.9^{+0.2}_{-0.2}$		120	1	1.1/77
	Medium	[0.07–0.33]	$3.6^{+0.6}_{-0.5}$	$1.6^{+0.2}_{-0.2}$		15	0.2	0.9/73
	Very low[e]	<0.07	$1.7^{+0.2}_{-0.0}$	$1.3^{+0.3}_{-0.3}$		0.5	0.005	614.3 (96.3)
	Very low[f]	<0.07	$0.3^{+0.3}_{-0.2}$	$0.5^{+0.3}_{-0.3}$	0.6 ± 0.3	0.6	0.006	598.9 (64.7)
IGR J17544−2619	High	>0.33	$1.7^{+0.3}_{-0.3}$	$1.4^{+0.2}_{-0.2}$		62	1	0.9/75
	Medium	[0.07–0.33]	$2.1^{+0.3}_{-0.3}$	$1.8^{+0.2}_{-0.2}$		14	0.3	1.0/72
	Very low[e]	<0.07	$1.1^{+0.1}_{-0.0}$	$2.2^{+0.3}_{-0.4}$		0.2	0.002	381.8 (83.0)
	Very low[f]	<0.07	$0.4^{+0.3}_{-0.3}$	$1.4^{+0.5}_{-0.4}$	0.2 ± 0.3	0.2	0.003	372.0 (53.1)
AX J1841.0−0536	High	>0.4	$2.5^{+0.3}_{-0.3}$	$1.1^{+0.1}_{-0.1}$		80	3	1.2/110
	Medium	[0.18–0.4]	$3.5^{+0.5}_{-0.5}$	$1.3^{+0.2}_{-0.2}$		34	1	1.1/102
	Low	[0.05–0.18]	$3.5^{+0.5}_{-0.5}$	$1.5^{+0.2}_{-0.2}$		11	0.4	1.2/104
	Very low[e]	<0.05	$0.3^{+0.3}_{-0.3}$	$0.6^{+0.4}_{-0.4}$	1.3 ± 1.0	0.6	0.02	449.5 (54.7)
Absorbed blackbody				kT_{bb}	Radius (km)			
IGR J16479−4514	High	>0.52	$4.2^{+0.5}_{-0.5}$	$1.9^{+0.1}_{-0.1}$	$0.54^{+0.06}_{-0.05}$	110	4	1.2/131
	Medium	[0.25–0.52]	$5.7^{+0.7}_{-0.6}$	$1.8^{+0.1}_{-0.1}$	$0.43^{+0.05}_{-0.04}$	51	2	1.1/132
	Low	[0.06–0.25]	$3.8^{+0.5}_{-0.4}$	$1.8^{+0.1}_{-0.1}$	$0.25^{+0.03}_{-0.02}$	17	0.6	1.0/144
	Very low[e]	<0.06	$3.3^{+0.5}_{-0.0}$	$1.2^{+0.2}_{-0.2}$	$0.14^{+0.05}_{-0.03}$	1.3	0.04	486.8 (99.5)
	Very low[f]	<0.06	$0.04^{+0.37}_{-0.04}$	$1.9^{+0.5}_{-0.4}$	$0.054^{+0.022}_{-0.001}$	1.4	0.04	462.4 (67.3)
XTE J1739−302	High	>0.33	$1.3^{+0.3}_{-0.2}$	$1.9^{+0.2}_{-0.1}$	$0.28^{+0.04}_{-0.03}$	100	1	1.3/77
	Medium	[0.07–0.33]	$1.5^{+0.3}_{-0.3}$	$1.5^{+0.1}_{-0.1}$	$0.16^{+0.02}_{-0.02}$	13	0.1	0.8/73
	Very low[e]	<0.07	$1.7^{+0.1}_{-0.0}$	$1.3^{+0.2}_{-0.1}$	$0.04^{+0.01}_{-0.01}$	0.5	0.004	646.1 (100.0)
	Very low[f]	<0.07	$0.0^{+0.1}_{-0.0}$	$1.7^{+0.3}_{-0.2}$	$0.022^{+0.005}_{-0.004}$	0.5	0.004	597.8 (49.8)
IGR J17544−2619	High	>0.33	$0.6^{+0.1}_{-0.1}$	$1.4^{+0.1}_{-0.1}$	$0.44^{+0.05}_{-0.04}$	53	0.9	1.3/75
	Medium	[0.07–0.33]	$0.8^{+0.2}_{-0.2}$	$1.2^{+0.1}_{-0.1}$	$0.30^{+0.04}_{-0.03}$	12	0.2	1.1/72
	Very low[e]	<0.07	$1.1^{+0.1}_{-0.0}$	$0.8^{+0.1}_{-0.1}$	$0.08^{+0.03}_{-0.02}$	0.2	0.002	425.9 (99.9)
	Very low[f]	<0.07	$0.0^{+0.1}_{-0.0}$	$1.1^{+0.2}_{-0.1}$	$0.04^{+0.01}_{-0.01}$	0.2	0.002	381.8 (50.5)
AX J1841.0−0536	High	>0.4	$1.2^{+0.2}_{-0.2}$	$1.7^{+0.1}_{-0.1}$	$0.51^{+0.05}_{-0.05}$	71	2	1.5/110
	Medium	[0.18–0.4]	$1.7^{+0.3}_{-0.3}$	$1.6^{+0.1}_{-0.1}$	$0.39^{+0.03}_{-0.03}$	30	1	1.2/102
	Low	[0.05–0.18]	$1.5^{+0.3}_{-0.2}$	$1.5^{+0.1}_{-0.1}$	$0.24^{+0.03}_{-0.02}$	9.9	0.3	1.0/104
	Very low[e]	<0.05	$0.0^{+0.1}_{-0.0}$	$1.7^{+0.4}_{-0.3}$	$0.04^{+0.01}_{-0.01}$	0.5	0.02	451.7 (50.0)

[a]Hardness ratio 4–10 keV/0.2–4 keV.
[b]Average observed 2–10 keV fluxes in units of 10^{-12} erg cm^{-2} s^{-1}.
[c]Average 2–10 keV X-ray luminosities in units of 10^{35} erg s^{-1} calculated adopting distances determined by Rahoui et al. (2008).
[d]Reduced χ^2 and dof, or Cash statistics Cstat and percentage of realizations (10^4 trials) with statistic >Cstat.
[e]Fit performed with constrained column density (see Section 5.2).
[f]Fit performed with free column density (see Section 5.2).

(and at least 1600 counts) in the ranges $CR_1 < CR < CR_2$ (low), $CR_2 < CR < CR_3$ (medium) and $CR > CR_3$ (high). If the statistics did not allow this, then we only considered two intensity levels (high and medium). Exposure maps were created for each of these intensity-selected event files. We then combined the intensity-selected event files (and their exposure maps) and extracted a single spectrum for each source by integrating over all the available observing time within these intensity limits. Ancillary response files were generated with XRTMKARF, and they account for different extraction regions, vignetting and PSF corrections. The spectra were rebinned with a minimum of 20 counts per energy bin to allow χ^2 fitting. Each spectrum was fit in the energy range 0.3–10 keV with a single absorbed power law, or an absorbed blackbody.

Downloaded from http://mnras.oxfordjournals.org/ at NASA Goddard Space Flight Ctr on July 1, 2014

Table 5. Observation log for IGR J16479−4514. This is a sample of the full table, which is available in the electronic version of the article – see Supporting Information.

Sequence	Instrument/mode	Start time (UT) (yyyy-mm-dd hh:mm:ss)	End time (UT) (yyyy-mm-dd hh:mm:ss)	Net exposure (s)
00030296005	XRT/PC	2007-10-26 08:08:36	2007-10-26 09:42:57	1176
00030296006	XRT/PC	2008-01-19 22:58:28	2008-01-19 23:13:58	927
00030296007	XRT/PC	2008-01-22 20:07:57	2008-01-22 20:25:58	1079
00030296008	XRT/PC	2008-01-26 18:56:04	2008-01-26 19:14:57	1133
00030296009	XRT/PC	2008-01-29 08:03:13	2008-01-29 08:20:56	1062

Table 6. Observation log for IGR J17391−3021. This is a sample of the full table, which is available in the electronic version of the article – see Supporting Information.

Sequence	Instrument/mode	Start time (UT) (yyyy-mm-dd hh:mm:ss)	End time (UT) (yyyy-mm-dd hh:mm:ss)	Net exposure (s)
00030987001	XRT/PC	2007-10-27 09:46:16	2007-10-27 10:05:57	1181
00030987002	XRT/PC	2007-10-30 10:12:32	2007-10-30 10:25:57	805
00030987003	XRT/PC	2007-11-01 08:47:14	2007-11-01 09:06:58	1181
00030987004	XRT/PC	2008-02-04 21:24:07	2008-02-04 22:57:58	940
00030987005	XRT/PC	2008-02-06 00:48:04	2008-02-06 23:29:58	5606

Table 7. Observation log for IGR J17544−2619. This is a sample of the full table, which is available in the electronic version of the article – see Supporting Information.

Sequence	Instrument/mode	Start time (UT) (yyyy-mm-dd hh:mm:ss)	End time (UT) (yyyy-mm-dd hh:mm:ss)	Net exposure (s)
00035056002	XRT/PC	2007-10-28 00:20:09	2007-10-29 07:07:56	2783
00035056003	XRT/PC	2007-10-31 10:19:05	2007-10-31 13:43:35	248
00035056004	XRT/PC	2007-11-04 00:58:32	2007-11-04 01:16:58	1104
00035056005	XRT/PC	2008-02-07 20:17:58	2008-02-07 23:43:57	1331
00035056006	XRT/PC	2008-02-10 19:14:07	2008-02-10 20:52:56	278

Table 8. Observation log for IGR J18410−0535. This is a sample of the full table, which is available in the electronic version of the article – see Supporting Information.

Sequence	Instrument/mode	Start time (UT) (yyyy-mm-dd hh:mm:ss)	End time (UT) (yyyy-mm-dd hh:mm:ss)	Net exposure (s)
00030988001	XRT/PC	2007-10-26 00:08:53	2007-10-26 06:45:56	1384
00030988002	XRT/PC	2007-10-28 22:53:11	2007-10-29 23:12:56	3199
00030988003	XRT/PC	2007-11-03 10:37:52	2007-11-03 12:24:56	1122
00030988004	XRT/PC	2007-11-05 09:08:39	2007-11-05 09:28:58	1218
00030988005	XRT/PC	2007-11-09 16:11:30	2007-11-09 16:32:56	1286

We also extracted spectra from the event list accumulated from all observations for which no detections were obtained as single exposures (very low). These spectra consisted of ∼100 counts each, so Cash (1979) statistics and spectrally unbinned data were used, instead. When fitting with free parameters, the best fitting value for $N_{\rm H}$ turned out to be consistent with 0, i.e. well below the column derived from optical spectroscopy. In this case, we performed further fits by adopting as lower limit on the absorbing column the value derived from the Galactic extinction estimate along the line of sight to each source from Rahoui et al. (2008), with a conversion into hydrogen column, $N_{\rm H} = 1.79 \times 10^{21} A_V$ cm^2 (Predehl & Schmitt 1995). As a comparison, we also report the simple hardness ratios.

The spectra and contour plots of photon index versus column density are shown in Figs 7 and 8, respectively, while the spectral parameters are reported in Table 4, where we also report the average 2–10 keV luminosities calculated by adopting distances determined by Rahoui et al. (2008) from optical spectroscopy of the supergiant companions (4.9 kpc for IGR J16479−4514, 2.7 kpc for XTE J1739−302 and 3.6 kpc for IGR J17544−2619). For AX J1841.0−0536, two estimates of the distance are available, (Nespoli, Fabregat & Mennickent 2008, $3.2^{+2.0}_{-1.5}$ kpc) and Sguera et al. (2009, 6.9 ± 1.7 kpc), and we assumed a distance of 5 kpc, which is consistent with both.

We note that spectral fits with an absorbed blackbody always result in blackbody radii of a few hundred metres (at the source distances, see Table 4 and Fig. 9), consistent with being emitted from a small portion of the neutron star surface, very likely the neutron star polar caps (Hickox, Narayan & Kallman 2004). Indeed, since SFXTs are wind accretors, alternative origins for the small emitting region, such as small hot regions in an accretion disc, can be discarded.

Downloaded from http://mnras.oxfordjournals.org/ at NASA Goddard Space Flight Ctr on July 1, 2014

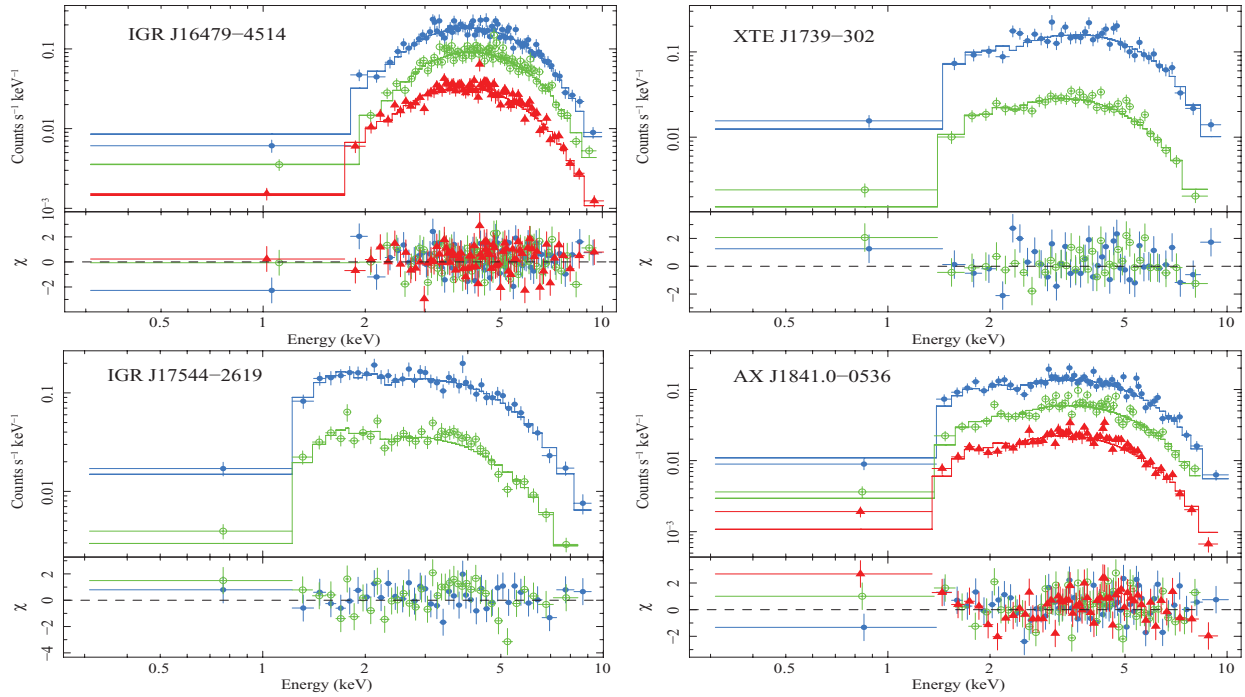

Figure 7. Spectroscopy of the 2007–2008 observing campaign. Upper panels: XRT/PC data fit with an absorbed power law. Lower panels: the residuals of the fit (in units of standard deviations). Filled blue circles, green empty circles and red filled triangles mark high, medium and low states, respectively.

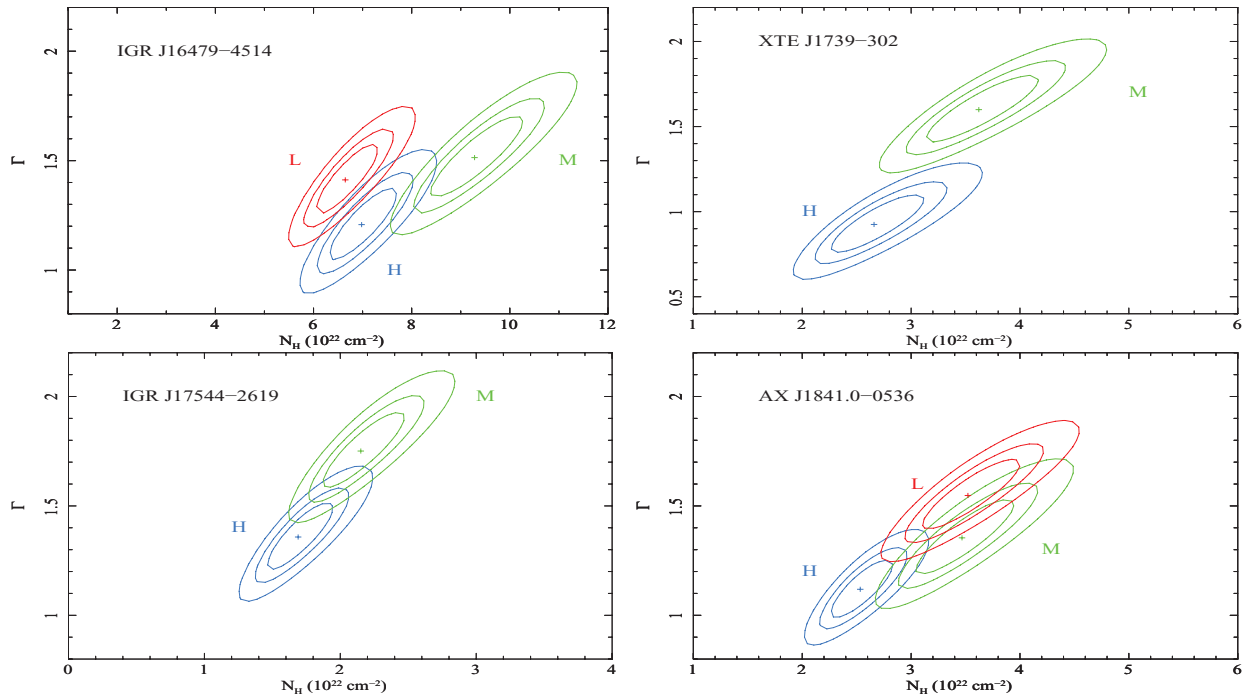

Figure 8. XRT time selected spectroscopy. The $\Delta\chi^2 = 2.3, 4.61$ and 9.21 contour levels for the column density in units of 10^{22} cm^{-2} versus the photon index, with best fits indicated by crosses. The colour scheme is the same as in Fig. 7. The labels L, M and H mark low, medium and high states, respectively.

6 DISCUSSION

We report on the results of an entire year of monitoring campaign with *Swift* of a subsample of SFXTs. For the first time, it is possible to investigate in depth the long-term properties of this new class of puzzling X-ray transients, assessing the characteristics of three different source states: the bright outbursts, the intermediate intensity state and the quiescence.

During this first year of monitoring, we have obtained multiwavelength observations of five outbursts of three different sources (see Table 1). As reported in Papers II, III and IV, we studied the broadband simultaneous spectra (0.3–150 keV) of three SFXTs. They can

Downloaded from http://mnras.oxfordjournals.org/ at NASA Goddard Space Flight Ctr on July 1, 2014

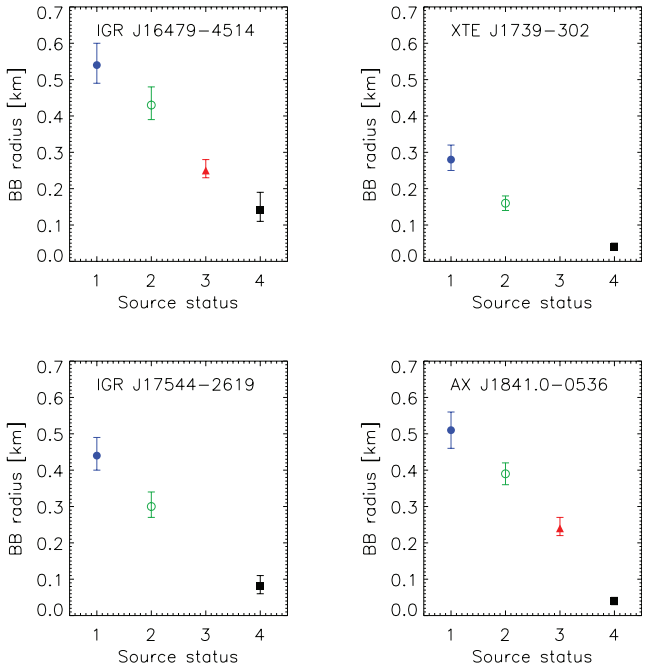

Figure 9. Blackbody radii as a function of source state. The colour coding is the same as in Figs 7 and 8. For the 'very low' state, we used the best fits with a constrained $N_{\rm H}$.

be fit with models traditionally adopted for accreting X-ray pulsars (absorbed cut-off power laws), even in the objects where proof of the presence of a neutron star (as derived from a spin period) is still unavailable. Considerable differences can be found in the behaviour of the absorbing column among the examined cases, and the new data from the 2009 January 29 outburst of IGR J16479−4514 fit well in this picture.

Our *Swift* monitoring campaign has demonstrated for the first time that X-ray emission from SFXTs is still present outside the bright outbursts, although at a much lower level (10^{33}–10^{34} erg s^{-1}). This was already emerging from the first 4 months of this campaign (Paper I), but now we have accumulated enough statistics to allow intensity selected spectroscopy of the out-of-outburst emission. Spectral fits performed adopting simple models, such as an absorbed power law or a blackbody (more complex models were not required by the data) result in hard power law photon indices (always in the range $\Gamma \sim 0.8$–2) or in hot black bodies ($kT_{\rm BB} \sim 1$–2 keV). It is remarkable that the statistics now accumulated allow us to constrain well the spectral parameters of the intermediate level of X-ray emission: in particular, when a blackbody model is adopted, the resulting radii of the emitter for all four SFXTs (and all the intensity states) is *always only* a few hundred metres (note that even with several kpc of uncertainty in the distance determination, the emitting regions are always significantly smaller than the neutron star radius). This is clearly indicative of an emitting region which is only a fraction of the neutron star surface, and can be associated in a natural way with the polar caps of the neutron star (Hickox et al. 2004). This evidence, coupled with the high level of flux variability and hard X-ray spectra, strongly supports the fact that the intermediate- and low-intensity level of SFXTs is produced by the accretion of matter onto the neutron star, demonstrating that SFXTs are sources which do not spend most of their lifetime in quiescence.

After following the X-ray light curves of the four SFXTs for 1 yr, we have obtained the first assessment of how long each source in our sample spends in each state using a systematic monitoring. The duty-cycle of inactivity is ∼17, 28, 39, 55 per cent (5 per cent uncertainty), for IGR J16479−4514, AX J1841.0−0536, XTE J1739–302 and IGR J17544−2619, respectively. For IGR J16479−4514 a contribution to the time spent in inactivity is due to the X-ray eclipses, hence the above 17 per cent is in fact an upper limit to the true quiescent time. In the latter three SFXTs, this inactivity duty cycle, where the sources are undetected with *Swift*, can be associated with the true quiescence (i.e. no accretion) and/or with an accretion at a very low rate. Thus, the quiescence in these transients is a rare state.

The lowest luminosity level we could monitor ('very low' intensity level in Table 4) with *Swift* is reached in XTE J1739–302 (6×10^{32} erg s^{-1}, 2–10 keV) and in IGR J17544−2619 (3×10^{32} erg s^{-1}). This latter value is consistent with the quiescent state observed in IGR J17544−2619 during a *Chandra* observation ($5.2 \pm 1.3 \times 10^{32}$ erg s^{-1}, 0.5–10 keV; in't Zand 2005), although the two spectra are very different. During the *Chandra* observation the spectrum was very soft, likely thermal (fitted with a power law resulted in a photon index $\Gamma = 5.9 \pm 1.2$), whereas our accumulated spectrum during the very low-intensity state is much harder ($\Gamma \sim 1$–2), very likely implying low-rate accretion onto the compact object. The lowest level of X-ray emission ever detected from XTE J1739–302 has been observed with *ASCA* (1.1×10^{-12} erg cm^{-2} s^{-1}, 2–10 keV; Sakano et al. 2002), which is much lower than that observed with *Swift*. This comparison, together with the hard spectrum and the small emitting radius (see Table 4) observed with *Swift* implies that we have not reached the quiescent state in this source. Besides IGR J17544−2619, the only other SFXTs where the quiescence (characterized by a soft thermal spectrum and a very low luminosity of $\sim 10^{32}$ erg s^{-1}) has been caught is IGR J08408–4503 (Leyder et al. 2007).

The low-intensity level we observe with *Swift* in IGR J16479−4514 is consistent with it being due to the X-ray eclipses. The possibility of an X-ray eclipse in this transient was originally suggested by Bozzo et al. (2008b), based on the variability of the iron line emission observed during an *XMM–Newton* observation. Then, Jain et al. (2009) found a periodicity at 3.32 d, suggesting it as a possible orbital period. We were able to confirm this periodicity from our independent analysis of the BAT data.

If we assume that this periodicity is of orbital origin, and consider a duration of the X-ray eclipse of 0.6 d (Jain et al. 2009), then the inclination i of the system can be derived from the eclipse semi-angle, θ_e, for an assumed supergiant radius ($R_{\rm OB} = 23.8\,{\rm R}_\odot$ for a O8.5 supergiant; Vacca, Garmany & Shull 1996) as $R_{\rm OB} = a\sqrt{(\cos^2 i + \sin^2 i \sin^2 \theta_e)}$. Assuming the system parameters previously adopted for IGR J16479–4514, we obtain a binary separation $a \approx 2 \times 10^{12}$ cm, implying an orbital inclination of $i \approx 40^\circ$.

This 3.32 d periodicity, if interpreted as the orbital period of the binary system, is puzzling, and is very difficult to reconcile with all the mechanisms proposed to explain the SFXTs phenomenon. The out-of-eclipse average X-ray luminosity of IGR J16479–4514 is $L_{\rm obs} \approx 10^{34}$–$10^{35}$ erg s^{-1}. It can be compared with the X-ray emission expected from Bondi–Hoyle accretion onto a neutron star. Let us assume a circular orbit (very likely, given the short period), a stellar mass of $M_{\rm OB} = 30\,{\rm M}_\odot$, a radius $R_{\rm OB} = 23.8\,{\rm R}_\odot$ for the supergiant (Vacca et al. 1996), a beta-law velocity for the supergiant wind $v(r) = v_\infty(1 - R_{\rm OB}/r)^\beta$ with $\beta = 1$, and a conservative high terminal velocity $v_\infty = 2000$ km s^{-1}. Under these assumptions, the X−ray luminosity produced by the wind accretion for a reasonable choice of the wind mass-loss rate ($\dot{M}_{\rm th} \approx 10^{-6}\,{\rm M}_\odot\,{\rm yr}^{-1}$) is $\sim 10^{37}$ erg s^{-1}, about 2–3 orders of magnitude higher than the observed luminosity. On the other hand, the observed low

Downloaded from http://mnras.oxfordjournals.org/ at NASA Goddard Space Flight Ctr on July 1, 2014

luminosity can be obtained only at a wind mass-loss rate of $\dot{M}_{\rm obs} \approx 10^{-8}$–$10^{-9}\,{\rm M}_{\odot}\,{\rm yr}^{-1}$, which is not reasonable for a O8.5 supergiant.

A viable explanation to this inconsistency could be that the 3.32 d periodicity is not orbital, but is only one of the periodicities predicted in our model for the explanation of SFXTs outbursts, that is the time interval between the periodically recurrent flares when the neutron star passes throughout the preferential plane for the outflowing wind from the supergiant, twice per orbit; thus, the true orbital period can be much longer than this periodicity found (see the different geometries proposed in Sidoli et al. 2007).

ACKNOWLEDGMENTS

We would like to thank our many collaborators, who helped along the way during this large project, and M. Colpi, who organized a 'Neutron Star Day' in Milano in 2006, during which so many new ideas came forth and unexpected collaborations were created. . . and who basically got this all started. Then, we would like to thank A. Bazzano, A. Cucchiara, S. Mereghetti, T. Mineo and P. Ubertini for helpful discussions. We thank the *Swift* team duty scientists and science planners P.J. Brown, M. Chester, S. Hunsberger, J. Racusin and M.C. Stroh for their dedication and willingness to accommodate our sudden requests in response to outbursts during this monitoring effort. We also thank the remainder of the *Swift* XRT and BAT teams, J.A. Nousek and S. Barthelmy in particular, for their invaluable help and support with the planning and execution of the observing strategy. This work was supported in Italy by contracts ASI I/088/06/0 and I/023/05/0, at PSU by NASA contract NAS5-00136. HAK was supported by the *Swift* project. DNB and JAK acknowledge support from NASA contract NAS5-00136. PR thanks INAF-IASF Milano and LS INAF-IASF Palermo, where some of the work was carried out, for their kind hospitality. We also thank the anonymous referee for comments that helped improve the paper.

Facility: *Swift*.

REFERENCES

Bamba A., Yokogawa J., Ueno M., Koyama K., Yamauchi S., 2001, PASJ, 53, 1179
Barthelmy S. D. et al., 2005, Space Sci. Rev., 120, 143
Blay P. et al., 2008, A&A, 489, 669
Bozzo E., Falanga M., Stella L., 2008a, ApJ, 683, 1031
Bozzo E., Stella L., Israel G., Falanga M., Campana S., 2008b, MNRAS, 391, L108
Burrows D. N. et al., 2005, Space Sci. Rev., 120, 165
Cash W., 1979, ApJ, 228, 939
Ducci L., Sidoli L., Paizis A., Mereghetti S., 2008, in Proc. 7th INTEGRAL Workshop, PoS(Integral08), 086, preprint (arXiv:0810.5463)
Gehrels N. et al., 2004, ApJ, 611, 1005
Hickox R. C., Narayan R., Kallman T. R., 2004, ApJ, 614, 881
Hill J. E. et al., 2005, Proc. SPIE, 5165, 217
in't Zand J. J. M., 2005, A&A, 441, L1
Jain C., Paul B., Dutta A., 2009, MNRAS, 397, L11
Krimm H. et al., 2006, Astron. Tel., 904
Krimm H. A. et al., 2007, Astron. Tel., 1265
Krimm H. A., Barthelmy S. D., Cummings J. R., Markwardt C. B., Skinner G., Tueller J., Swift/BAT Team, 2008, in AAS/High Energy Astrophysics Division, Vol. 10, Status of the Swift/BAT Hard X-ray Transient Monitor. American Astron. Soc., Los Angeles, p. 07.01
Krimm H. A., Romano P., Sidoli L., 2009, Astron. Tel., 1971
La Parola V. et al., 2009, Astron. Tel., 1929
Leyder J.-C., Walter R., Lazos M., Masetti N., Produit N., 2007, A&A, 465, L35
Negueruela I., Smith D. M., Harrison T. E., Torrejón J. M., 2006, ApJ, 638, 982
Negueruela I., Torrejón J. M., Reig P., Ribó M., Smith D. M., 2008, in AIP Conf. Ser. Vol. 1010, A Population Explosion: The Nature & Evolution of X-ray Binaries in Diverse Environments. Am. Inst. Phys., New York, p. 252
Nespoli E., Fabregat J., Mennickent R. E., 2008, A&A, 486, 911
Poole T. S. et al., 2008, MNRAS, 383, 627
Predehl P., Schmitt J. H. M. M., 1995, A&A, 293, 889
Rahoui F., Chaty S., Lagage P.-O., Pantin E., 2008, A&A, 484, 801
Romano P., Sidoli L., Mangano V., Mereghetti S., Cusumano G., 2007, A&A, 469, L5
Romano P. et al., 2008a, Astron. Tel., 1697
Romano P. et al., 2008b, Astron. Tel., 1659
Romano P. et al., 2008c, ApJ, 680, L137 (Paper II)
Romano P. et al., 2009a, Astron. Tel., 1961
Romano P. et al., 2009b, Astron. Tel., 1920
Roming P. W. A. et al., 2005, Space Sci. Rev., 120, 95
Sakano M., Koyama K., Murakami H., Maeda Y., Yamauchi S., 2002, ApJS, 138, 19
Sguera V. et al., 2005, A&A, 444, 221
Sguera V. et al., 2007, A&A, 467, 249
Sguera V., Romero G. E., Bazzano A., Masetti N., Bird A. J., Bassani L., 2009, ApJ, 697, 1194
Sidoli L., 2009, Adv. Space Res., 43, 1464
Sidoli L., Romano P., Mereghetti S., Paizis A., Vercellone S., Mangano V., Götz D., 2007, A&A, 476, 1307
Sidoli L. et al., 2008, ApJ, 687, 1230 (Paper I)
Sidoli L. et al., 2009a, MNRAS, 397, 1528 (Paper IV)
Sidoli L. et al., 2009b, ApJ, 690, 120 (Paper III)
Smith D. M., Main D., Marshall F., Swank J., Heindl W. A., Leventhal M., in 't Zand J. J. M., Heise J., 1998, ApJ, 501, L181
Swank J. H., Smith D. M., Markwardt C. B., 2007, Astron. Tel., 999
Vacca W. D., Garmany C. D., Shull J. M., 1996, ApJ, 460, 914
Vaughan S. et al., 2006, ApJ, 638, 920
Walter R., Zurita Heras J., 2007, A&A, 476, 335

SUPPORTING INFORMATION

Additional Supporting Information may be found in the online version of this article:

Table 5. Observation log for IGR J16479−4514.
Table 6. Observation log for IGR J17391−3021.
Table 7. Observation log for IGR J17544−2619.
Table 8. Observation log for IGR J18410−0535.

Please note: Wiley-Blackwell are not responsible for the content or functionality of any supporting information supplied by the authors. Any queries (other than missing material) should be directed to the corresponding author for the article.

This paper has been typeset from a TEX/LATEX file prepared by the author.

Downloaded from http://mnras.oxfordjournals.org/ at NASA Goddard Space Flight Ctr on July 1, 2014